Conformation of the Cell Division Regulator MinE: Evidence for Interactions between the Topological Specificity and Anti-MinCD Domains†

Dennis Ramos,‡ Thierry Ducat,‡ Jenny Cheng,§ Nelson F. Eng,§ Jo-Anne R. Dillon,§,|| and Natalie K. Goto*,‡,§

Department of Chemistry and Department of Biochemistry, Microbiology, and Immunology, University of Ottawa, Ottawa, Ontario, Canada K1N 6N5

Received January 5, 2006; Revised Manuscript Received February 15, 2006

ABSTRACT: Symmetric division of Gram-negative bacteria depends on the combined action of three proteins that ensure correct positioning of the cell division septum, namely, MinC, MinD, and MinE. To achieve this function, MinC and MinD form a membrane-bound complex that blocks cell division at all potential sites. Opposing this inhibition is MinE, which interacts with MinD via its N-terminal anti-MinCD domain to site-specifically counter the action of the MinCD complex. The anti-MinCD domain has been proposed to bind MinD in a helical conformation; however, little is actually known about the structure of this functionally critical region. To understand how MinE can perform its anti-MinCD function, we have therefore investigated the conformation of the full-length MinE from *Neisseria gonorrhoeae* by solution NMR. Although solubility considerations required the use of sample conditions that limit the observation of amide resonances to regions that are protected from solvent exchange, backbone chemical shifts from both N- and C-terminal domains could be assigned. In contrast to previous models, secondary chemical shift analysis of these solvent-protected regions shows that parts of the N-terminal anti-MinCD domain are stably folded with many functionally important residues localizing to a β-structure. In addition, this N-terminal domain may be interacting with the C-terminal topological specificity domain, since mutations made in one domain led to NMR spectral changes in both domains. The nonfunctional MinE mutant L22D showed even larger evidence of structural perturbations in both domains, with significant destabilization of the entire MinE structure. Overall, these results suggest that there is an intimate structural association between the anti-MinCD and topological specificity domains, allowing the functional properties of the two domains to be modulated through this interaction.

Precise regulation of cell division is critical to the viability of prokaryotic and eukaryotic cells. To ensure that equal amounts of genetic material are distributed between daughter cells, it is necessary that they divide symmetrically. This means that the cytokinetic septum that splits the cell must be formed at the appropriate location. In rod-shaped bacteria such as *Escherichia coli*, this occurs at the cell midpoint in a plane perpendicular to the long axis of the cell (*1*), while in round bacteria such as *Neisseria gonorrhoeae*, division occurs centrally along alternating perpendicular planes (*2*, *3*). For both cell types placement of the cell division site is determined, in part, by the presence of the nucleoid, which inhibits formation of the FtsZ polymer that is key for septation (*4*, *5*). However, additional factors are required to ensure that the cell division septum does not localize to nonmidpoint regions of the cell not occluded by the nucleoid (*6*−*9*). In Gram-negative bacteria, this is achieved by the action of three proteins encoded by the *minB* operon, namely, MinC, MinD, and MinE (*6*, *10*, *11*).

Although the pattern of cell division in the two cell types is different, studies with Min proteins from the bacillus *E. coli* and the coccus *N. gonorrhoeae* suggest that they perform analogous functions to ensure proper placement of the cell division plane (*12*, *13*). In both cases MinD and MinC localize to a polymeric subcellular coiled structure on the membrane at one end of the cell, creating a zone that is inhibitory to formation of the cytokinetic septum (*14*, *15*). This MinCD-rich region expands along the subcellular scaffold over time, extending toward the midcell whereupon it is thought to disperse to cluster at the opposite pole of the cell and establish a new MinCD zone (*16*−*18*). Coordinated with MinCD oscillation is a concentrated membrane-associated annulus of MinE (called the E-ring) that also oscillates back and forth along the polymeric array between the polar regions, lagging behind MinC and MinD (*12*, *14*, *19*−*21*). The presence of the E-ring appears to ensure that time-averaged concentrations of the inhibitory MinCD complex will be lowest at the midcell, creating a central zone permissive to septum formation (*8*, *17*, *20*, *22*).

Underlying the oscillatory movement of Min proteins in the cell is an ATP-dependent cycle of interactions between MinD and MinE or MinC. In this cycle, MinC inhibits

† This work was supported by start-up funds from the University of Ottawa Faculty Development Fund. N.F.E. was funded by a Natural Sciences and Engineering Research Council (NSERC) Doctoral Canada Graduate Scholarship.

* To whom correspondence should be addressed. Tel: (613) 562-5800 ext 6918. Fax: (613) 562-5170. E-mail: Natalie.Goto@science.uottawa.ca.

‡ Department of Chemistry, University of Ottawa.

§ Department of Biochemistry, Microbiology, and Immunology, University of Ottawa.

|| Current address: Department of Biology, College of Arts and Science, University of Saskatchewan, Saskatoon, SK, Canada S7N 5A5.

10.1021/bi060022j CCC: $33.50
Published on Web 03/17/2006

septation by interacting with FtsZ to induce disassembly of the cytokinetic FtsZ polymer (*23*−*25*). However, to perform this function, MinC must be targeted to the membrane via interactions with MinD, which cooperatively associates with the membrane when bound to ATP (*26*−*29*). MinC inhibition of cell division is alleviated when its interaction with MinD is disrupted by MinE, which binds to an overlapping site on MinD (*30*, *31*). This interaction with MinE also promotes the intrinsic ATPase activity of MinD (*32*, *33*), causing the dissociation of MinD from the membrane and release of MinE (*26*, *27*, *29*).

The region of the *E. coli* MinE (Ec-MinE)[1] responsible for MinD interactions has been localized to an N-terminal 31-residue segment (called the anti-MinCD domain) which binds to MinD and dissociates the MinCD complex, allowing cell division to occur (*34*). Even when an N-terminal fragment is expressed in place of full-length MinE, MinCD activity is inhibited and cell division can proceed (*30*, *35*). However, in this case cell division can occur both at midcell and at the poles of *E. coli*, suggesting that the missing C-terminal portion is required to impart topological specificity to MinE function. Truncation analyses and mutagenesis studies have shown that this topological specificity function of MinE is retained in a structural domain that encompasses residues 34−88 in the *E. coli* protein (called the topological specificity domain, or TSD) (*34*−*36*). Solution NMR studies of this domain from Ec-MinE established that it forms an independently folded dimeric $\alpha\beta$ structure (*37*). In contrast, solution NMR of a 22-residue N-terminal Ec-MinE peptide suggests that it does not form a stable independent fold, although it may possess nascent helix structure (*36*). Consequently, it has been proposed that the anti-MinCD domain exists in a largely disordered conformation that is primed for interactions with MinD (*37*).

While many studies have established the fact that anti-MinCD function can be decoupled from topological specificity by the expression of isolated MinE domains, evidence is available for MinE from *N. gonorrhoeae* that mutations made to the TSD can have an impact on MinD-binding activity (*38*). The observation that mutations in one domain can alter the functional properties normally attributed to the other domain therefore raises the possibility that there are interactions between domains modulating their respective structural and functional properties. However, no structural information from a full-length MinE protein is available that could establish the conformation of the two functional domains as they would exist in the intact protein. To investigate the possibility of structural interdependence of the two MinE domains, we have therefore studied full-length MinE from the round bacterium *N. gonorrhoeae* using solution NMR and circular dichroism spectroscopy.

EXPERIMENTAL PROCEDURES

Sample Preparation. All Ng-MinE samples with a C-terminal hexahistidine tag were prepared using the previously described plasmids pEC1 for wild-type, pEA18D for A18D, and pEL22D for the L22D mutant Ng-MinE (*38*). The E46A mutant was generated using the QuikChange site-directed mutagenesis kit as described by the manufacturer (Stratagene) using pEC1 with the following set of complementary primers synthesized by Integrated DNA Technologies Inc.: $^{5'}$CCTGCCGACTTTACGTAAAGCGTTGATGGAAGTCCTGTCC$^{3'}$ and $^{5'}$GGACAGGACTTCCATCAACGCTTTACGTAAAGTCGGCAGG$^{3'}$. The identity of all constructs was confirmed by sequencing performed at the Ontario Genomics Innovation Centre at the Ottawa Health Research Institute.

All Ng-MinE constructs were prepared using a slightly modified version of the previously published protocol (*38*). Briefly, one colony of freshly transformed BL21(DE3) was used to inoculate 50 mL of M9 minimal media containing 50 μg/mL kanamycin and 0.1% (w/v) ^{15}N-labeled ammonium chloride and 0.3% (w/v) glucose (either U-^{13}C or natural abundance) as the sole nitrogen and carbon sources, respectively. The culture was grown overnight at 37 °C and used to inoculate 1 L of the same minimal media which was induced with 0.4 mM isopropyl β-D-thiogalactopyranoside when the OD_{600} reached 0.6−0.8. Cells were harvested by centrifugation 3 h after induction, and the pellet from each 1 L culture was resuspended in 30 mL of 20 mM sodium phosphate buffer, pH 8.0, with 10 mM imidazole and 500 mM NaCl. Lysozyme (500 μg/mL) was added prior to lysis by sonication, and the insoluble material was pelleted by centrifugation. After the supernatant was passed through a 2 μm filter, it was applied to a 1 mL His-Trap column using an AKTA FPLC and washed with 10 mL of the same buffer followed by 15 mL of this buffer supplemented with 100 mM imidazole. A 100−500 mM imidazole gradient was then run over a 5 mL volume in the same buffer, and Ng-MinE eluted as a single peak at approximately 400 mM imidazole. Fractions containing Ng-MinE were dialyzed against 50 mM Tris, pH 9.5, 50 mM NaCl, and 1 mM EDTA and concentrated using 5K MWCO Amicon Ultra centrifugal filter units to yield samples that were >95% pure as determined by Coomassie-stained SDS−PAGE. For circular dichroism and size exclusion experiments the concentrated samples were further purified on a Superdex-75 10/300 GL column in the same buffer, and only the main peak corresponding to dimeric MinE was collected and concentrated for further study.

NMR Spectroscopy. All NMR spectra were recorded at the Quebec/Eastern Canada High Field NMR Facility on the cryoprobe-equipped INOVA 500 or at the University of Ottawa NMR Facility on the INOVA 500. Spectra were recorded at 25 °C in 50 mM Tris, 50 mM NaCl, 100 μM EDTA, 0.02% sodium azide, 0.2 mM phenylmethanesulfonyl fluoride, and 10% D_2O, processed by NMRPipe (*39*), and analyzed with NMRView (*40*). Ng-MinE concentrations were typically ~0.9−1.5 mM for spectra recorded at pH 9.5 and 100 μM for the wild-type spectrum recorded at pH 7.8. All HSQC spectra shown, including that of L22D, were reproduced at least once with proteins produced from independent purifications and found to yield superimposable spectra.

Backbone ^{15}N, $^{1}H^{N}$, $^{13}C_{\alpha}$, $^{13}C_{\beta}$, and ^{13}CO chemical shift assignments were made on the wild-type Ng-MinE at pH 9.5 based on HNCACB, CBCA(CO)NH, HNCA, HN(CO)CA, and HNCO experiments, and amide proton assignments

[1] Abbreviations: Ec-MinE, *Escherichia coli* MinE; Ng-MinE, *Neisseria gonorrhoeae* MinE; TSD, topological specificity domain; Ec- or Ng-TSD, *E. coli* or *N. gonorrhoeae* topological specificity domain; CD, circular dichroism; HSQC, heteronuclear single-quantum coherence; NOE, nuclear Overhauser effect; NOESY, NOE spectroscopy; EDTA, ethylenediaminetetraacetic acid; SDS−PAGE, sodium dodecyl sulfate−polyacrylamide gel electrophoresis.

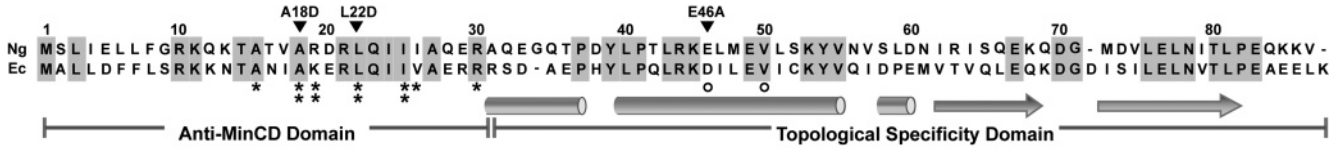

FIGURE 1: Primary sequence of MinE from *N. gonorrhoeae* (Ng) aligned with the *E. coli* (Ec) homologue. Identity is 42% as highlighted in the sequence. Mutants investigated in the current study are shown above the sequence, with sequence numbering reflecting that of Ng-MinE. Highly conserved amino acids that were previously identified to be important for MinD binding (*46*, *48*) are indicated with asterisks, with the number of asterisks reflecting the relative impact of mutations made at these positions on anti-MinCD function. Residues previously identified to be important for E-ring formation (*22*) are also specified with open dots. The secondary structure previously determined for the Ec-TSD (*37*) is schematically displayed below the Ec-MinE sequence.

were confirmed with a ^{15}N-edited NOESY utilizing a 100 ms mixing time (*41*, *42*). Protected regions were mapped onto the Ec-TSD structure (*37*; PDB accession number 1EV0), and figures were rendered in MolMol (*43*). ^{1}H, ^{13}C, and ^{15}N chemical shifts were referenced using a 2,2-dimethyl-2-silapentane-5-sulfonate internal standard, and secondary shifts from peptide-derived random coil values were calculated using NMRView. Although only Cα secondary shifts are shown, secondary shifts for Cβ and CO atoms were also calculated and found to agree very closely with those from Cα atoms.

Circular Dichroism Spectroscopy. All samples for circular dichroism (CD) spectroscopy were prepared by dialysis of purified wild-type or mutant Ng-MinE samples into 10 mM Tris buffer at either pH 7.4 or pH 9.5. CD spectra were recorded on a Jasco J-810 circular dichroism spectropolarimeter with a 0.1 mm path length quartz cell at 25 °C. Spectra reflect an average of eight scans recorded from 250 to 190 nm with a 0.2 nm step resolution, a speed of 20 nm/min, and a bandwidth of 1.0 nm. CD spectra were found to be reproducible for all samples over a concentration range of 10−100 μM under both pH conditions. Following CD spectroscopy, the concentration of the samples used to calculate the molar ellipticity per mean residue was determined using a modified version of the Bradford assay and confirmed using the BCA assay, and the structural integrity was confirmed by SDS−PAGE analysis.

RESULTS

Backbone Amide Protons in Ng-MinE Are Protected from Solvent Exchange at High pH. In our structural investigation of a full-length bacterial MinE protein we chose to focus on MinE from *N. gonorrhoeae* to complement our previous functional analyses on Min proteins from round bacteria (*6*, *12*, *13*, *15*, *38*, *44*). For this purpose we used a C-terminally hexahistidine-tagged Ng-MinE construct that could be expressed and purified in high yield from *E. coli* in ^{15}N- and ^{15}N,^{13}C-isotopically labeled forms. Since the C-terminus of Ng-MinE does not appear to be critical to MinE structure or function (*38*), the His tag was not removed for these studies. Functional assays for Ng-MinD with this tagged Ng-MinE construct confirm that this construct retains the ability to promote a >10-fold increase in MinD ATPase activity similar to observations made with the *E. coli* proteins (data not shown).

To evaluate the structural state of purified Ng-MinE, ^{1}H−^{15}N correlation HSQC NMR spectra can be recorded, providing a fingerprint spectrum for the backbone amide protons. In this experiment, peak intensity is favored by solution conditions that minimize the rate of amide proton exchange with solvent, which is typically in the pH range of 5−7. However, we found that Ng-MinE was poorly soluble when the pH of the solution dropped below ~8.0 in a wide range of tested buffers. The highest concentration that could be obtained within the desired pH range was 50 μM at pH 7.0, although this sample tended to slowly precipitate over time. Conversely, Ng-MinE could be concentrated to much higher levels when the pH of the solution was greater than 8.0, with a concomitant improvement in sample stability. Since a stably folded protein will possess hydrogen-bonded and/or buried backbone amide protons that would be protected from rapid solvent exchange, it can be possible to observe signals from these amide protons in the ^{1}H−^{15}N HSQC spectrum at high pH. Therefore, to determine whether Ng-MinE was folded under conditions where it was soluble, we recorded a ^{1}H−^{15}N HSQC spectrum of a 1.5 mM ^{15}N-labeled sample at pH 9.5. As shown by the red spectrum in Figure 2A, 47 of the expected 89 peaks are observed, indicating that approximately half of the amide protons are protected from rapid solvent exchange. In addition, the wide range of proton chemical shifts demonstrates that the regions resistant to solvent exchange comprise part of a folded domain, as would be expected from the solvent protection.

To establish that the structure of Ng-MinE at high pH is similar to its structure at a more physiological pH, a 100 μM ^{15}N-labeled sample of Ng-MinE was also prepared at pH 7.8. The HSQC spectrum of this sample (Figure 2A, black spectrum) shows the appearance of approximately 20 new backbone amide proton peaks that are distinct from those observed in the high-pH spectrum that likely arise from parts of MinE that are only partially protected from solvent exchange. In addition, a subset of peaks was obtained that overlaps exactly with those in the high-pH spectrum. Since chemical shift is a property that is highly sensitive to the local chemical environment, the absence of pH-dependent chemical shift changes in these peaks shows that the core of the structure of Ng-MinE is not altered by high-pH conditions. The absence of a structural change upon varying solution pH conditions was further substantiated by circular dichroism spectroscopy, which showed superimposable spectra for Ng-MinE in the two pH conditions (data not shown).

To identify the parts of Ng-MinE that are resistant to solvent exchange at high pH, backbone chemical shift resonances were assigned for 45 of the 47 peaks at pH 9.5. Thirty of the assigned residues could be mapped onto homologous regions in the NMR structure of the TSD from Ec-MinE (Figure 2B). This analysis showed that the regions of Ng-MinE that are protected from solvent exchange occur

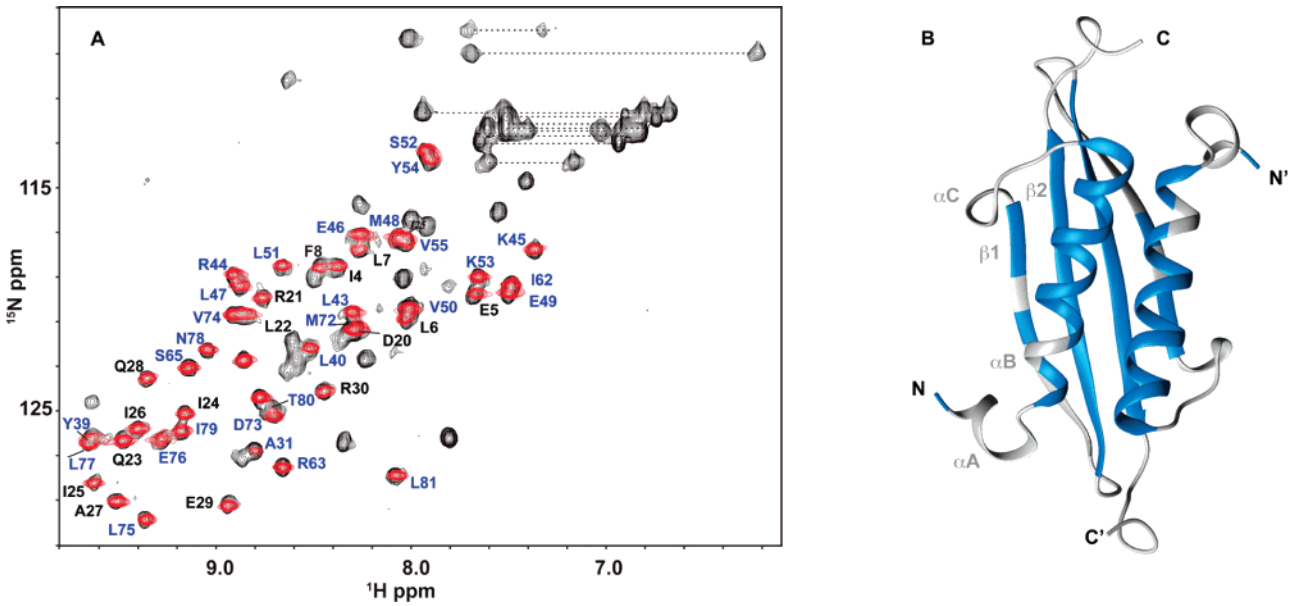

FIGURE 2: Ng-MinE contains stable structure in both N- and C-terminal domains at high pH. (A) Assigned ^{1}H−^{15}N HSQC spectrum of wild-type MinE at pH 9.5 (in red) superimposed on the pH 7.8 spectrum (in black). Residues assigned to the anti-MinCD domain are labeled in black. TSD residues are indicated in blue and have been mapped onto the ribbon diagram of the TSD structure (B) previously determined for Ec-MinE (*37*).

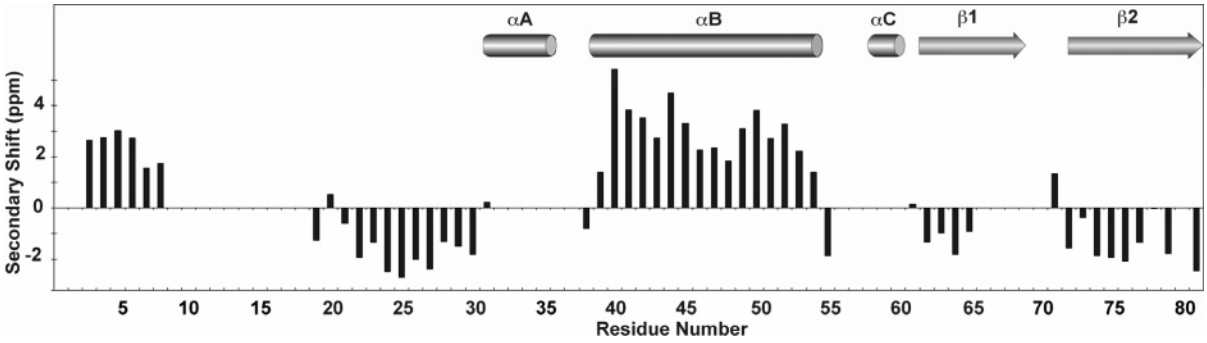

FIGURE 3: Secondary structure of Ng-MinE determined from secondary Cα chemical shifts. Shown are the differences between experimental Cα chemical shifts and published random coil values (*45*) for Ng-MinE at pH 9.5. Regions showing positive secondary Cα shifts indicate a helical conformation, while negative secondary shifts are characteristic of *β*-structures. Residues not visible in the NMR spectrum at this pH were not assigned and have been given a secondary shift value of zero. Secondary structure elements for homologous regions from Ec-TSD as defined in the previously determined NMR structure (*37*) are shown schematically.

in the central α-helix (αB) and *β*-sheet (*β*2) that form the extensive dimeric interface between monomers in addition to the N-terminal half of the outermost *β*-sheet (*β*1). The remaining peaks were assigned to two regions in the N-terminal anti-MinCD domain encompassing residues 4−8 and 20−30.

Secondary Structure of Ng-MinE. From assigned backbone chemical shift resonances it is possible to obtain a reliable prediction of secondary structure by calculating secondary shifts (defined as the difference between experimental and random coil values) (*45*). The results of this analysis for backbone Cα shifts are shown in Figure 3. Positive secondary shifts indicative of helical conformations were observed for residues homologous to the helical regions previously determined in the Ec-TSD structure, while negative secondary shifts characteristic of *β*-structure arose in regions homologous to strands *β*1 and *β*2. The agreement between secondary shift predictions and the Ec-TSD structure conforms to the expectation that the high sequence similarity between the Ec- and Ng-MinE proteins (Figure 1) should give rise to similar structures.

The predicted secondary structure of the assigned N-terminal domain residues is of particular interest since no structural information for a full-length anti-MinCD domain was previously available. As shown in Figure 3, significant positive secondary shifts are observed for residues 3−8, which would suggest that this part of the N-terminal domain is helical. In addition to the N-terminal helix, anti-MinCD residues 21−30 show secondary shifts that predict for a *β*-conformation. Secondary structures identified in both N-terminal and C-terminal domains were confirmed in a ^{15}N-NOESY experiment by the presence of significant correlations between amide protons of consecutive residues for helices (Supporting Information, Figure S1). For *β*-strand residues these NOE correlations were very weak, as would be expected due to the larger distance separating consecutive amide protons in this conformation.

Evidence for Interactions between MinE N- and C-Terminal Domains. The presence of structure in the N-terminal domain of Ng-MinE raises the possibility that the two functional domains of this protein may interact with each other. To explore this possibility, ^{15}N-labeled samples were

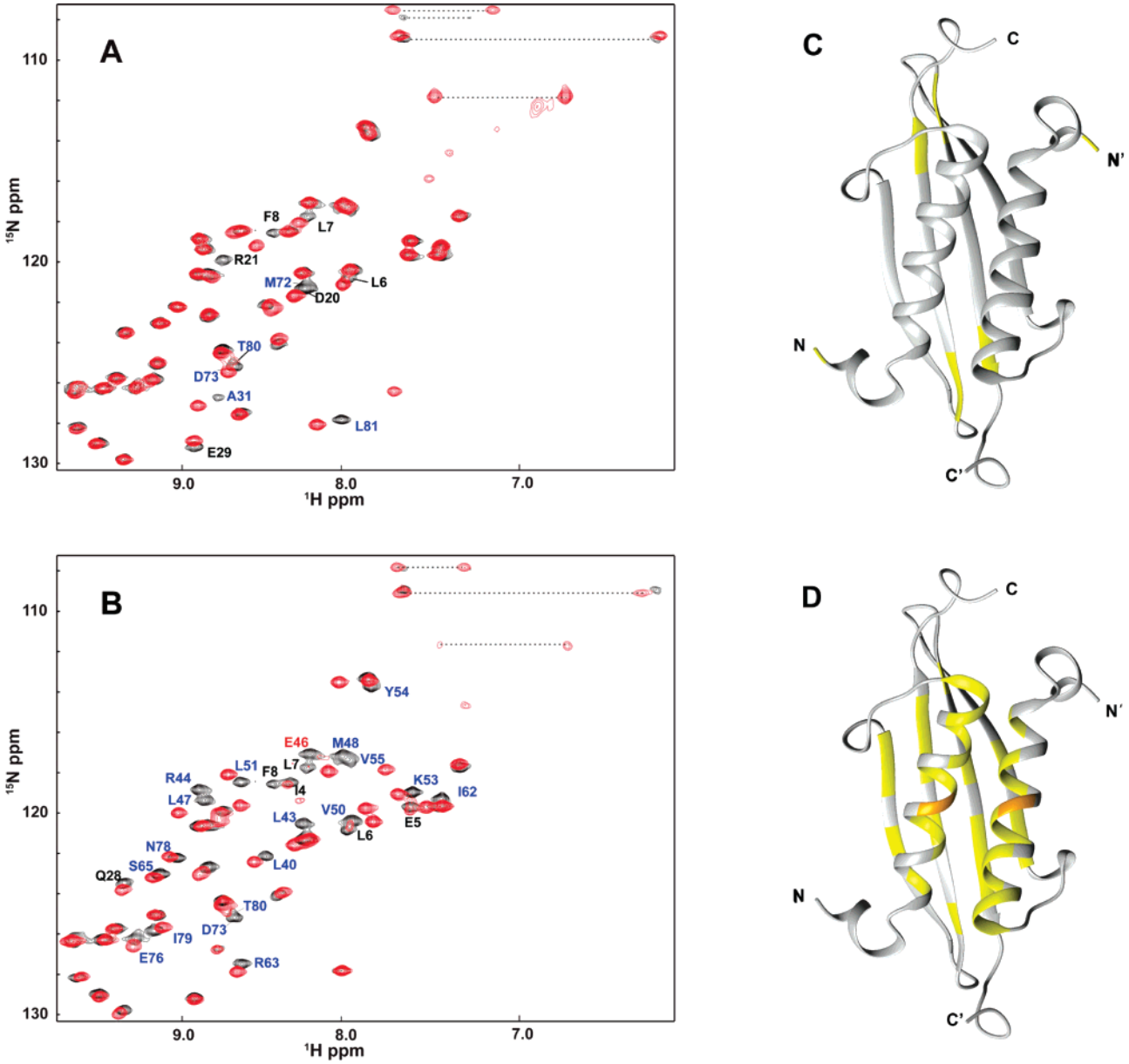

FIGURE 4: Mutations in Ng-MinE lead to chemical shift changes in both TSD and anti-MinCD domains. ^{1}H−^{15}N HSQC spectra of MinE mutants A18D (A) and E46A (B) are shown in red superimposed on the black spectrum of wild-type MinE. All spectra were recorded at pH 9.5, 25 °C. TSD peaks in the wild-type spectrum that are not reproduced in the mutant spectrum are labeled in blue and also highlighted in yellow in the ribbon structure for the Ec-TSD (C, D). E46 is highlighted in orange in (D).

made of Ng-MinE that contained a mutation in either the N-terminal domain (A18D) or the C-terminal domain (E46A). These mutations are also of functional interest since A18D Ng-MinE cannot bind MinD (*38*) and E46 has been shown to be important for E-ring formation in Ec-MinE (*22*, *37*). As shown in Figure 4A, the HSQC spectrum of the A18D mutant (in red) shows only small differences from the spectrum recorded for wild-type Ng-MinE (black), suggesting that no large-scale structural changes are introduced by the mutation. Circular dichroism spectra of wild-type and A18D Ng-MinE indicate that the secondary structure content has not been changed by this mutation (Figure 5A), providing additional evidence that the overall structure of the two proteins is similar. However, from the HSQC spectrum it appears that the local chemical environment of some residues has been altered by the mutation since some peaks in the wild-type spectrum, including those for N-terminal residues L6−F8, D20, R21, E29 and A31, are not reproduced in the A18D spectrum. In addition, Ng-TSD residues M72, D73, T80, and L81 also show differences between the two spectra. Localization of the corresponding residues in the Ec-TSD structure illustrates that they are clustered together at the dimer interface between the central two β-strands at two equivalent sites (Figure 4C). The identification of a region of the Ng-TSD that is sensitive to mutations made to the anti-MinCD domain indicates that these C-terminal residues must experience a change in local chemical environment, potentially via an interaction between N- and C-terminal domains.

The HSQC spectrum of the E46A mutant revealed more extensive, larger scale chemical shift perturbations relative to the wild-type spectrum (Figure 4B), as would be expected from the close proximity of this TSD α-helix residue to the dimerization interface. Previous studies with Ec-TSD suggested that the analogous mutation does not perturb its global structure (*37*), in agreement with the CD spectrum for the

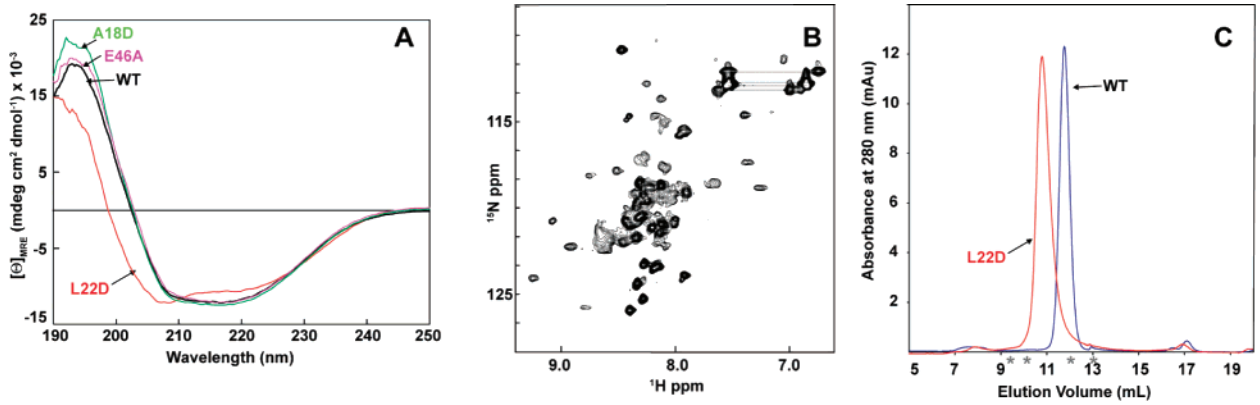

FIGURE 5: Mutation of Leu22 destabilizes Ng-MinE structure. (A) Circular dichroic spectra of MinE wild-type (black), E46A (purple), A18D (green), and L22D (red) mutant proteins in 10 mM Tris, pH 7.4. Protein concentrations were 15−20 μM. (B) ^{1}H−^{15}N HSQC spectrum of the 250 μM L22D mutant recorded at pH 7.2, 25 °C. (C) Size exclusion profile for 100 μM wild-type and L22D Ng-MinE run on a Superdex-75 column in 50 mM Tris, pH 9.5, 150 mM NaCl, and 1 mM EDTA. The elution profiles for both proteins were found to be the same over a wide range of concentrations (10−250 μM). Elution volumes of molecular mass standards are indicated with asterisks (from left to right: albumin, 67 kDa; ovalbumin, 43 kDa; chymotrypsinogen A, 25 kDa; ribonuclease A, 13.7 kDa).

Ng-MinE E46A mutant, which is superimposable with that of the wild-type protein (Figure 5A). While the HSQC spectrum of the E46A mutant shows that many peaks are unaffected by the mutation, a number of peaks in the wild-type spectrum were not reproduced in the mutant spectrum. These include peaks from residues along the length of the central helix responsible for packing interactions between subunits and β-sheet residues that pack against this helix (Figure 4D). Apart from these changes in the TSD resonances, residues in the N-terminal helix also showed the effect of the E46A mutation, with L7 and F8 showing the most notable difference since no trace of peak intensity at the wild-type position was observed for these peaks in the mutant spectrum. In addition, I4, E5, and L6 all appear to be broadened in the E46A spectrum. Again, this observation that mutations made in the C-terminal domain of Ng-MinE are sensed in the N-terminal domain supports the possibility that the two domains are structurally associated.

The structure of another N-domain mutant known to disrupt anti-MinCD function, namely, L22D (*38*), was also investigated by NMR and CD (Figure 5). In contrast to the other mutants, the CD spectrum of L22D showed a significant difference from the wild-type spectrum, with a small decrease in helix and increase in random coil contributions (<∼5% change) according to secondary structure deconvolution programs. This difference in structure was confirmed in the HSQC, which showed no amide peaks at high pH despite high solubility. Therefore, L22D appears to lack a stable structure that could protect backbone amides from solvent exchange. This was substantiated by the HSQC run under neutral pH conditions (Figure 5B) which revealed a mixture of peaks of strong intensity and poor chemical shift dispersion characteristic of unfolded proteins and broad peaks over a larger chemical shift range that may reflect regions of residual structure undergoing intermediate time-scale exchange processes. It is not likely that the broadening is due to aggregation since size exclusion chromatography showed that this mutant elutes as a single peak with an elution volume that is slightly less than that of the wild-type (Figure 5C). It should be noted that it is not possible to ascertain the oligomerization state of L22D from this analysis since unfolded extended states are less compact than folded globular states, which would lead to faster relative mobility in gel filtration chromatography. Overall, these results provide strong evidence that the L22D mutation affects the structure and stability of the full-length protein even though the site of mutation in the primary sequence is far from the C-terminal domain and the TSD dimerization interface.

DISCUSSION

In order for bacterial cell division to exclusively occur at midcell, MinE must counteract the inhibitory action of the MinCD complex site-specifically. For this purpose it performs two functional roles: MinD binding to dissociate the MinCD complex and MinE ring formation to ensure topological specificity. It has been shown that these two functions can be decoupled by expressing fragments of MinE, with N-terminal fragments being associated with anti-MinCD activity and C-terminal fragments disrupting topological specificity (*34*, *35*). Although the study of these functional domains in isolation has led to the identification of a number of functionally critical residues (*37*, *46*), this approach does not permit the detection of functional changes that may arise due to the influence of the other domain. In addition, no structural study had yet been performed on a MinE sample containing the full 30 residues from the N-terminal domain, giving rise to models of MinE function that are partially based on structural predictions for this domain. Therefore, to better understand the structural properties of the N-terminal domain, we studied the conformation of the full-length Ng-MinE using NMR and CD spectroscopy.

Assignment of peaks in the high-pH ^{1}H−^{15}N HSQC spectrum of Ng-MinE showed that regions that are protected from solvent exchange correspond to sequences that are homologous to α- and β-secondary structure elements in the previously determined structure of the Ec-TSD (*37*). In addition, N-terminal anti-MinCD domain residues were also clearly evident in the spectrum, establishing that parts of this domain are folded in the intact protein. Initially, this was a surprising result given that a previous trypsin digest performed on full-length Ec-MinE showed that only the C-terminal domain is resistant to digestion, implying that the N-terminal domain might not be folded (*36*). However, we observe that almost all of the potential sites for trypsin cleavage in the N-terminal domain lie outside the protected

regions that are visible in our spectra. The NMR solvent accessibility results on Ng-MinE therefore correlate well with previous trypsin digestion studies on Ec-MinE since these solvent-accessible regions are more likely to be cleaved. Cleavage at one or more of these sites would likely disrupt the ability of the N-terminal region to fold, thereby facilitating complete digestion of this domain. Hence it is likely that the structure detected in the N-terminal domain of Ng-MinE is a conserved feature that is also present in the *E. coli* protein.

Additional confirmation of the structural similarity between the Ec- and Ng-MinE proteins was provided by our secondary chemical shift calculations. The secondary structure obtained for protected residues in the Ng-TSD corresponds exactly to the Ec-TSD solution NMR structure. Similar results were also obtained for the first solvent-protected segment at the N-terminus of Ng-MinE. The α-helical conformation observed for this segment in full-length Ng-MinE corresponds to the same region of Ec-MinE that displayed helix-specific NOEs in a 22-residue N-terminal Ec-MinE peptide (Ec-$MinE_{1-22}$) (*36*). Therefore, the secondary shifts suggest a high degree of structural similarity between Ec- and Ng-MinE proteins. This structural homology was also predicted previously from cross-species complementation studies showing that Ng-MinE can oscillate in *E. coli* when expressed with Ec-MinD and that oscillation of Ng-MinD can be induced in *E. coli* by coexpression with either Ng-MinE or Ec-MinE (*12*). Since Min proteins from the two species can function together in vivo, it is likely that these homologues have closely related structures and act via similar mechanisms. This is additionally substantiated by previous studies demonstrating that mutations made to residues that are important for anti-MinCD function in Ec-MinE have a similar impact on Ng-MinE function (*38*, *46*). Given the high degree of sequence homology between Ec- and Ng-MinE (Figure 1), as well as the structural and functional similarity, we anticipate that the structural properties of Ng-MinE will prove to be highly similar for MinE proteins in general.

Our investigations on mutants of Ng-MinE raised the possibility that interactions occur between the two functional domains since mutations in one domain led to spectroscopic changes in the other domain. It is of interest to note that the N-terminal helix peaks were affected for both A18D and E46A mutants, which may reflect a direct role for this helix in interdomain interactions. This possibility could explain why deletion of five residues from the N-terminal side of Ec-MinE in vivo leads to cell length heterogeneity and some minicell formation (*35*). Given that this helix does not appear to participate in direct interactions with MinD according to protein interaction studies in yeast on Ng-MinE (*38*) and Ec-$MinE_{1-31}$ (*46*), deletion of the first five residues may instead disrupt an interdomain interaction that is important for regulating topological specificity. While the details behind this interaction have yet to be resolved, one possibility to consider is that deletion of this helix may alter the accessibility of residues important for MinD binding and/or topological specificity.

Additional evidence supporting an interaction between anti-MinCD and TS domains was provided by our analysis of the Ng-MinE mutant L22D. Like the A18D mutant, L22D is not able to bind to Ng-MinD or induce oscillation in *E. coli* (*38*). However, in contrast to A18D, both NMR and CD spectra for this mutant show evidence of destabilization and partial unfolding. This shows that even when a mutation is introduced that is far from the structured TSD, the structural properties of both domains of Ng-MinE can be altered. This would suggest that the two functional domains are not structurally independent, a factor that must be considered when interpreting the impact of mutations on MinE activity.

Our proposal that the anti-MinCD domain interacts with the TSD would help to explain why MinE does not independently localize to the membrane even though the anti-MinCD domain by itself has a tendency to bind the *E. coli* inner membrane. For example, GFP-tagged N-terminal Ec-MinE peptide ($MinE_{1-31}$) has been shown to localize to the membrane even when MinD is not present (*46*). However, if the N-terminal domain is folded together with the TSD in the full-length protein, it would be inaccessible for membrane binding. A disruption of this interaction would explain why mutants L22S, L22R, or I25R in full-length Ec-MinE exhibit MinD-independent membrane localization (*46*). As we observed for the L22D mutant of Ng-MinE, the structure and stability of these mutants may be dramatically different from wild-type, with the N-terminal domain being available for promiscuous membrane interactions.

One of the most interesting findings from our studies was that residues 20−30 of the *N. gonorrhoeae* anti-MinCD domain are in a β-conformation. Previous models of MinE-MinD interactions had suggested that this region should be α-helical when bound to MinD (*36*, *37*). This idea was corroborated by yeast two-hybrid experiments with a 31-residue N-terminal fragment of Ec-MinE that identified anti-MinCD residues important for MinD binding (*46*). These residues were shown to localize to one face of a hypothetical α-helix, potentially giving rise to a continuous MinD-binding surface (*46*). However, our results indicate that, in the absence of MinD, many of these critical anti-MinCD residues (e.g., L22, I25, I26, R30) are located in a structured region that is clearly in a β-conformation.

The periodicity of a typical β-sheet structure ensures that the side chain from every other residue will be located on one side of the sheet. However, the residues that have been identified as important in the MinD−MinE interaction (Figure 1) do not display this periodicity and would therefore be predicted to localize to both sides of an ideal β-sheet. Although the current data cannot be used to establish whether this region does form an ideal β-sheet uninterrupted by turns, another possibility to consider is that only a subset of these residues directly participates in the MinD interaction, with the others being critical to the structural integrity of MinE. Our results with L22D provide support for this scenario since disruption of the anti-MinCD β-strand had a significant impact on the structural properties of the whole protein. The MinD-independent membrane localization of the I25R Ec-MinE mutant (*46*) indicates a similar role for I25 in the full-length protein. It is also worthy to note that anti-MinCD function is retained by Ec-$MinE_{1-22}$, a fragment that does not contain many of the residues subsequently identified as important for MinD interactions (*34*). This suggests that the minimum region required for interaction with MinD is provided by the first 22 residues and that the β-strand region may be important for other functions, such as stabilization of the structure of MinE.

Additional insight into the structural role of this anti-MinCD domain β-region has been provided by previous studies with N-terminal truncations of Ec-MinE that explored the involvement of this segment in MinE dimerization (*47*). Although it is clear from structural and biophysical investigations that the TSD is capable of dimerization without the anti-MinCD domain (*36*, *37*), this study showed that residues in the anti-MinCD domain can contribute to the interaction. Specifically, when expressed together with wild-type MinE in vivo, Ec-MinE$_{22-87}$ was found to form heterodimers with the full-length wild-type protein, while the shorter Ec-MinE$_{31-87}$ fragment did not. Since only the MinE mutant that contained the anti-MinCD β-region was found to interact with the full-length protein in these studies, this region may be responsible for unique interdomain interactions that enhance dimerization affinity. These additional cross-subunit interactions might also increase the stability of the full-length protein, potentially explaining the dramatic effect that mutations in this region can have on MinE structure.

Cross-subunit interactions mediated by the N-terminal domain of MinE could also provide a potential explanation of how topological specificity can be conferred. From previous studies, it appears that normal cell division requires that a concentrated zone of MinCD must oscillate between poles along a subcellular coiled array (*14*, *15*) and that high concentrations of MinE localize to the leading edge of the MinCD zone to form the E-ring (*8*, *14*, *21*). Mutations in Ec-MinE such as D45A/V49A that have lost topological specificity also do not show evidence of E-ring formation, giving rise to longer MinCD polar zones with irregular growth and decay properties (*22*). On the basis of these results it was suggested that E-ring formation involves interactions between the TSD and either other parts of MinE or other proteins yet to be identified. Our finding suggesting that the TSD interacts with the anti-MinCD domain of MinE raises the possibility that these interactions may even occur between MinE dimers. Similar to "domain swapping" where intramolecular interactions are exchanged for intermolecular interactions, a low-affinity MinE oligomerization could be facilitated by interactions where intradimer interactions between the anti-MinCD and topological specificity domains are replaced by interdimer interactions. In fact, sedimentation equilibrium experiments on purified Ec-MinE indicate that low-affinity tetramer and octamer formation does occur (*47*) but is not observed for the TSD alone (*36*). Given that the local concentration of MinE that is incorporated into the coiled array could be very high, formation of these higher order oligomers may be favored in this case. The role of the TSD in the formation of these higher order structures could explain the requirement for this domain in normal bacterial cell division. However, it is clear that understanding how MinE performs its anti-MinCD function site-specifically will require high-resolution structural information on the full-length protein, a prospect which is currently being pursued in our laboratories. This not only will clarify how the anti-MinCD domain can bind to MinD but also should provide insight into how the TSD contributes to the interaction and how topological specificity is conferred.

ACKNOWLEDGMENT

We thank Dr. Tito Scaiano for allowing access to his CD spectrometer and Larisa Mikelsons for assisting with its operation.

SUPPORTING INFORMATION AVAILABLE

^{1}H$-^1$H strip plots from the amide region of the ^{15}N-NOESY from wild-type Ng-MinE at pH 9.5. This material is available free of charge via the Internet at http://pubs.acs.org.

REFERENCES

1. Nanninga, N. (1998) Morphogenesis of *Escherichia coli*, *Microbiol. Mol. Biol. Rev. 62*, 110−129.
2. Westling-Haggstrom, B., Elmros, T., Normark, S., and Winblad, B. (1977) Growth pattern and cell division in *Neisseria gonorrhoeae*, *J. Bacteriol. 129*, 333−342.
3. Fitz-James, P. (1964) Thin sections of dividing *Neisseria gonorrhoeae*, *J. Bacteriol. 87*, 1477−1482.
4. Yu, X. C., and Margolin, W. (1999) FtsZ ring clusters in min and partition mutants: role of both the Min system and the nucleoid in regulating FtsZ ring localization, *Mol. Microbiol. 32*, 315−326.
5. Mulder, E., and Woldringh, C. L. (1989) Actively replicating nucleoids influence positioning of division sites in *Escherichia coli* filaments forming cells lacking DNA, *J. Bacteriol. 171*, 4303−4314.
6. Ramirez-Arcos, S., Szeto, J., Beveridge, T. J., Victor, C., Francis, F., and Dillon, J. A. R. (2001) Deletion of the cell-division inhibitor MinC results in lysis of *Neisseria gonorrhoeae*, *Microbiology 147*, 225−237.
7. Adler, H. I., Fisher, W. D., Cohen, A., and Hardigree, A. A. (1967) Miniature *Escherichia coli* cells deficient in DNA, *Proc. Natl. Acad. Sci. U.S.A. 57*, 321−326.
8. Raskin, D. M., and de Boer, P. A. J. (1997) The MinE ring: an FtsZ-independent cell structure required for selection of the correct division site in *E. coli*, *Cell 91*, 685−694.
9. Yu, X. C., Sun, Q., and Margolin, W. (2001) FtsZ rings in mukB mutants with or without the Min system, *Biochimie 83*, 125−129.
10. De Boer, P. A. J., Crossley, R. E., and Rothfield, L. I. (1988) Isolation and properties of minB, a complex genetic locus involved in correct placement of the division site in *Escherichia coli*, *J. Bacteriol. 170*, 2106−2112.
11. De Boer, P. A. J., Crossley, R. E., and Rothfield, L. I. (1989) A division inhibitor and a topological specificity factor coded for by the minicell locus determine proper placement of the division septum in *E. coli*, *Cell 56*, 641−649.
12. Ramirez-Arcos, S., Szeto, J., Dillon, J. A. R., and Margolin, W. (2002) Conservation of dynamic localization among MinD and MinE orthologues: oscillation of *Neisseria gonorrhoeae* proteins in *Escherichia coli*, *Mol. Microbiol. 46*, 493−504.
13. Szeto, J., Acharya, S., Eng, N. F., and Dillon, J. A. R. (2004) The N terminus of MinD contains determinants which affect its dynamic localization and enzymatic activity, *J. Bacteriol. 186*, 7175−7185.
14. Shih, Y. L., Le, T., and Rothfield, L. (2003) Division site selection in *Escherichia coli* involves dynamic redistribution of Min proteins within coiled structures that extend between the two cell poles, *Proc. Natl. Acad. Sci. U.S.A. 100*, 7865−7870.
15. Szeto, J., Eng, N. F., Acharya, S., Rigden, M. D., and Dillon, J. A. R. (2005) A conserved polar region in the cell division site determinant MinD is required for responding to MinE-induced oscillation but not for localization within coiled arrays, *Res. Microbiol. 156*, 17−29.
16. Raskin, D. M., and de Boer, P. A. J. (1999) MinDE-dependent pole-to-pole oscillation of division inhibitor MinC in *Escherichia coli*, *J. Bacteriol. 181*, 6419−6424.
17. Raskin, D. M., and de Boer, P. A. J. (1999) Rapid pole-to-pole oscillation of a protein required for directing division to the middle of *Escherichia coli*, *Proc. Natl. Acad. Sci. U.S.A. 96*, 4971−4976.
18. Corbin, B. D., Yu, X. C., and Margolin, W. (2002) Exploring intracellular space: function of the Min system in round-shaped *Escherichia coli*, *EMBO J. 21*, 1998−2008.

19. Margolin, W. (2001) Bacterial cell division: a moving MinE sweeper boggles the MinD, *Curr. Biol. 11*, R395−R398.
20. Hale, C. A., Meinhardt, H., and de Boer, P. A. J. (2001) Dynamic localization cycle of the cell division regulator MinE in *Escherichia coli*, *EMBO J. 20*, 1563−1572.
21. Fu, X. L., Shih, Y. L., Zhang, Y., and Rothfield, L. I. (2001) The MinE ring required for proper placement of the division site is a mobile structure that changes its cellular location during the *Escherichia coli* division cycle, *Proc. Natl. Acad. Sci. U.S.A. 98*, 980−985.
22. Shih, Y. L., Fu, X. L., King, G. F., Le, T., and Rothfield, L. (2002) Division site placement in *E. coli*: mutations that prevent formation of the MinE ring lead to loss of the normal midcell arrest of growth of polar MinD membrane domains, *EMBO J. 21*, 3347−3357.
23. Bi, E., and Lutkenhaus, J. (1993) Cell division inhibitors SulA and MinCD prevent formation of the FtsZ ring, *J. Bacteriol. 175*, 1118−1125.
24. Hu, Z. L., and Lutkenhaus, J. (1999) Topological regulation of cell division in *Escherichia coli* involves rapid pole to pole oscillation of the division inhibitor MinC under the control of MinD and MinE, *Mol. Microbiol. 34*, 82−90.
25. Justice, S. S., Garcia-Lara, J., and Rothfield, L. I. (2000) Cell division inhibitors SulA and MinC/MinD block septum formation at different steps in the assembly of the *Escherichia coli* division machinery, *Mol. Microbiol. 37*, 410−423.
26. Lackner, L. L., Raskin, D. M., and de Boer, P. A. J. (2003) ATP-dependent interactions between *Escherichia coli* Min proteins and the phospholipid membrane in vitro, *J. Bacteriol. 185*, 735−749.
27. Hu, Z. L., Gogol, E. P., and Lutkenhaus, J. (2002) Dynamic assembly of MinD on phospholipid vesicles regulated by ATP and MinE, *Proc. Natl. Acad. Sci. U.S.A. 99*, 6761−6766.
28. Mileykovskaya, E., Fishov, I., Fu, X. Y., Corbin, B. D., Margolin, W., and Dowhan, W. (2003) Effects of phospholipid composition on MinD-membrane interactions in vitro and in vivo, *J. Biol. Chem. 278*, 22193−22198.
29. Suefuji, K., Valluzzi, R., and RayChaudhuri, D. (2002) Dynamic assembly of MinD into filament bundles modulated by ATP, phospholipids, and MinE, *Proc. Natl. Acad. Sci. U.S.A. 99*, 16776−16781.
30. Ma, L. Y., King, G. F., and Rothfield, L. (2004) Positioning of the MinE binding site on the MinD surface suggests a plausible mechanism for activation of the *Escherichia coli* MinD ATPase during division site selection, *Mol. Microbiol. 54*, 99−108.
31. Zhou, H. J., Schulze, R., Cox, S., Saez, C., Hu, Z. L., and Lutkenhaus, J. (2005) Analysis of MinD mutations reveals residues required for MinE stimulation of the MinD ATPase and residues required for MinC interaction, *J. Bacteriol. 187*, 629−638.
32. De Boer, P. A. J., Crossley, R. E., Hand, A. R., and Rothfield, L. I. (1991) The MinD protein is a membrane ATPase required for the correct placement of the *Escherichia coli* division site, *EMBO J. 10*, 4371−4380.
33. Lutkenhaus, J., and Sundaramoorthy, M. (2003) MinD and role of the deviant Walker A motif, dimerization and membrane binding in oscillation, *Mol. Microbiol. 48*, 295−303.
34. Zhao, C. R., de Boer, P. A. J., and Rothfield, L. I. (1995) Proper placement of the *Escherichia coli* division site requires two functions that are associated with different domains of the MinE protein, *Proc. Natl. Acad. Sci. U.S.A. 92*, 4313−4317.
35. Pichoff, S., Vollrath, B., Touriol, C., and Bouche, J. P. (1995) Deletion analysis of gene minE which encodes the topological specificity factor of cell division in *Escherichia coli*, *Mol. Microbiol. 18*, 321−329.
36. King, G. F., Rowland, S. L., Pan, B., Mackay, J. P., Mullen, G. P., and Rothfield, L. I. (1999) The dimerization and topological specificity functions of MinE reside in a structurally autonomous C-terminal domain, *Mol. Microbiol. 31*, 1161−1169.
37. King, G. F., Shih, Y. L., Maciejewski, M. W., Bains, N. P. S., Pan, B. L., Rowland, S. L., Mullen, G. P., and Rothfield, L. I. (2000) Structural basis for the topological specificity function of MinE, *Nat. Struct. Biol. 7*, 1013−1017.
38. Eng, N. F., Szeto, J., Acharya, S., Tessier D., and Dillon J. A. R. (2005) The C-terminus of MinE from *Neisseria gonorrhoeae* acts as a topological specificity factor by modulating MinD activity in bacterial cell division, *Res. Microbiol.* (in press).
39. Delaglio, F., Grzesiek, S., Vuister, G. W., Zhu, G., Pfeifer, J., and Bax, A. (1995) NMRPipe: a multidimensional spectral processing system based on UNIX pipes, *J. Biomol. NMR 6*, 277−293.
40. Johnson, B. A., and Blevins, R. A. (1994) NMRView: A computer program for the visualization and analysis of NMR data, *J. Biomol. NMR 4*, 603−614.
41. Kanelis, V., Forman-Kay, J. D., and Kay, L. E. (2001) Multidimensional NMR methods for protein structure determination, *IUBMB Life 52*, 291−302.
42. Sattler, M., Schleucher, J., and Griesinger, C. (1999) Heteronuclear multidimensional NMR experiments for the structure determination of proteins in solution employing pulsed field gradients, *Prog. Nucl. Magn. Res. Spectrosc. 34*, 93−158.
43. Koradi, R., Billeter, M., and Wuthrich, K. (1996) MOLMOL: a program for display and analysis of macromolecular structures, *J. Mol. Graphics 14*, 51−55.
44. Szeto, J., Ramirez-Arcos, S., Raymond, C., Hicks, L. D., Kay, C. M., and Dillon, J. A. R. (2001) Gonococcal MinD affects cell division in *Neisseria gonorrhoeae* and *Escherichia coli* and exhibits a novel self-interaction, *J. Bacteriol. 183*, 6253−6264.
45. Wishart, D. S., Sykes, B. D., and Richards, F. M. (1992) The chemical shift index: a fast and simple method for the assignment of protein secondary structure through NMR spectroscopy, *Biochemistry 31*, 1647−1651.
46. Ma, L. Y., King, G., and Rothfield, L. (2003) Mapping the MinE site involved in interaction with the MinD division site selection protein of *Escherichia coli*, *J. Bacteriol. 185*, 4948−4955.
47. Zhang, Y., Rowland, S., King, G., Braswell, E., and Rothfield, L. (1998) The relationship between hetero-oligomer formation and function of the topological specificity domain of the *Escherichia coli* MinE protein, *Mol. Microbiol. 30*, 265−273.
48. Hu, Z. L., and Lutkenhaus, J. (2001) Topological regulation of cell division in *E. coli.* Spatiotemporal oscillation of MinD requires stimulation of its ATPase by MinE and phospholipids, *Mol. Cell 7*, 1337−1343.

BI060022J